JACS
JOURNAL OF THE AMERICAN CHEMICAL SOCIETY
pubs.acs.org/JACS
Article

Structural Plasticity as a Driver of the Maturation of Pro-Interleukin-18

Jeffrey P. Bonin,* James M. Aramini, and Lewis E. Kay*

Cite This: J. Am. Chem. Soc. 2024, 146, 30281−30293
Read Online
ACCESS | Metrics & More | Article Recommendations | Supporting Information

ABSTRACT: Dynamics are often critical for biomolecular function. Herein we explore the role of motion in driving the maturation process of pro-IL-18, a potent pro-inflammatory cytokine that is cleaved by caspases-1 and -4 to generate the mature form of the protein. An NMR dynamics study of pro-IL-18, probing time scales over 12 orders of magnitude and focusing on ^{1}H, ^{13}C, and ^{15}N spin probes along the protein backbone and amino-acid side chains, reveals a plastic structure, with millisecond time scale dynamics occurring in a pair of β-strands, $\beta1$ and β^*, that show large structural variations in a comparison of caspase-free and bound pro-IL-18 states. Fits of the relaxation data to a three-site model of exchange showed that the ground state secondary structure is maintained in the excited conformers, with the side chain of I48 that undergoes a buried-to-exposed conformational change in the caspase-free to -bound transition of pro-IL-18, sampling a more extensive range of torsion angles in one of the excited states characterized, suggesting partial unpacking in this region. Hydrogen exchange measurements establish the occurrence of an additional process, whereby strands $\beta1$ and β^* locally unfold. Our data are consistent with a hierarchy of dynamic events that likely prime pro-IL-18 for facile caspase binding.

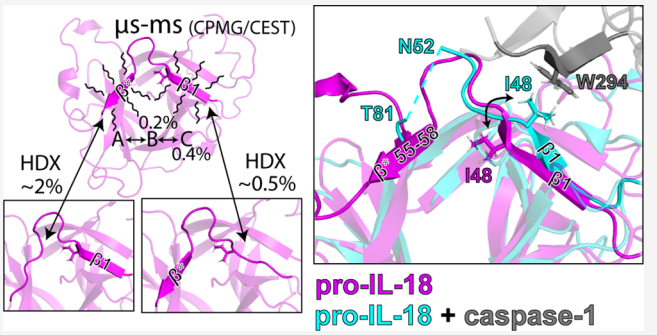

INTRODUCTION

Proteins are dynamic molecules that interconvert between different conformational states on a wide range of time scales.[1,2] The often sparsely populated, transiently formed structures that result have been shown to play integral roles in protein function, including in allostery, molecular interactions, and enzyme catalysis.[3−8] Examples, among the many that are notable, include work by the Kalodimos group establishing the importance of rare conformers of Abl kinase in explaining the mechanism by which some mutations confer resistance to imatinib, a kinase inhibitor targeting Bcr-Abl for the treatment of chronic myelogenous leukemia,[9] and studies by the Kern laboratory showing that protein dynamics can direct enzyme function in a variety of systems.[10,11] In particular, protein dynamics can also serve to guide the evolution of structure. For example, Wright and co-workers have shown that in *E. coli* dihydrofolate reductase, each intermediate of the multistep catalytic cycle samples sparse conformations that closely resemble the ground state structure of the adjacent intermediate(s) in the cycle.[12] In addition, Beach et al. have demonstrated that apo RNaseA populates a conformation similar to the structure of the substrate bound enzyme.[3] Further, Culik et al. have established that the immature form of SOD1 explores conformations resembling those of the ground state structures of subsequent steps of its maturation pathway and that the conformational space available to the molecule becomes increasingly restricted as maturation proceeds.[13] We present here a further example, involving a small signaling protein, interleukin-18 (IL-18), whose dynamics in the pro-form may play a significant role in facilitating its maturation process.

As a member of the interleukin-1 cytokine family, IL-18 is a key player in regulating innate immunity and inflammation.[14] IL-18 is expressed in an inactive form, termed pro-IL-18, with an N-terminal pro-domain (residues 1−36) and a C-terminal mature domain (residues 37−193). Proteolytic cleavage, primarily by the inflammatory caspases caspase-1 and caspase-4,[15,16] removes the pro domain, thus producing the mature (active) form of the protein (Figure 1a). Mature IL-18 is then secreted, leading to its subsequent binding to an IL-18 receptor localized to the surface of either the cell from which it originated or neighboring immune cells, such as T-cells and dendritic cells,[15,17] ultimately resulting in the production of interferon-γ that, in turn, plays an important role in modulating

Received: July 18, 2024
Revised: October 11, 2024
Accepted: October 14, 2024
Published: October 24, 2024

https://doi.org/10.1021/jacs.4c09805
J. Am. Chem. Soc. 2024, 146, 30281−30293

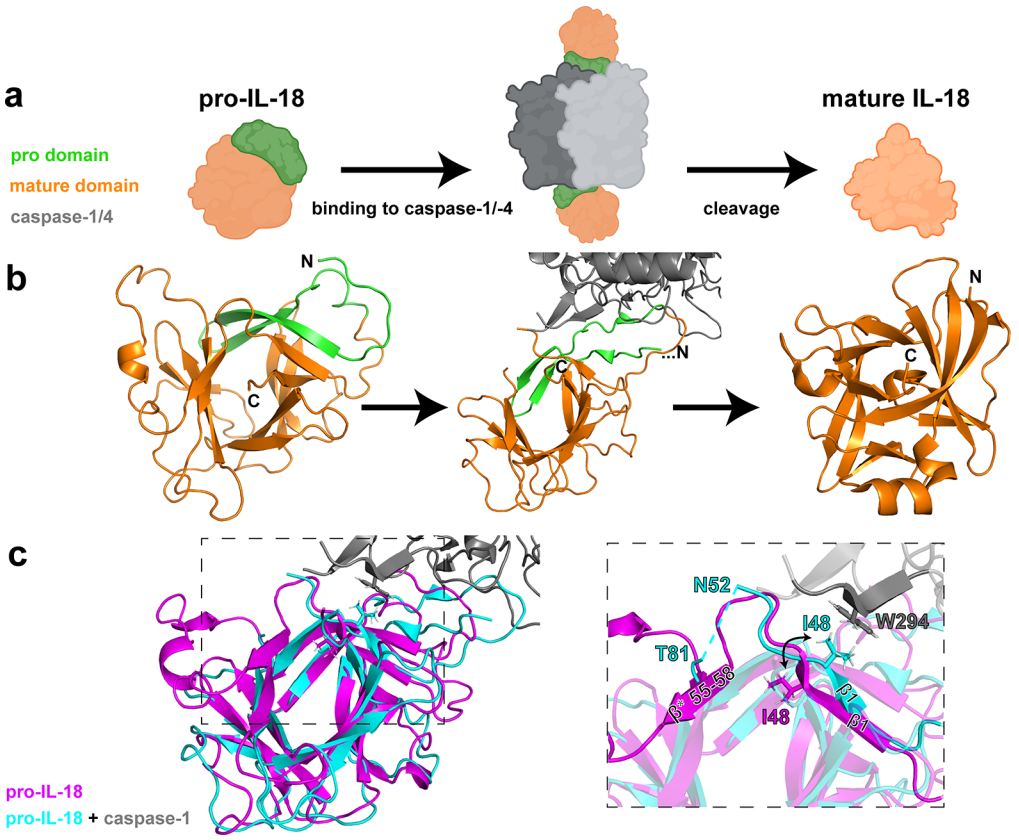

Figure 1. Maturation of IL-18 requires structural changes. (a) Cartoon representation of IL-18 maturation. Pro-IL-18, containing a pro-domain (green) and a mature domain (orange), binds to caspase-1/-4 (gray). Caspase-1/-4 then cleaves pro-IL-18, removing the pro-domain and producing the mature cytokine. Note that the binding stoichiometry is two pro-IL-18:two caspase-1/-4. (b) Structures of IL-18 at each step of the maturation process are shown (pro-IL-18:8URV, pro-IL-18 + caspase-1:8SV1, mature IL-18:3WO2). The color scheme is the same as that in (a). N- and C-termini are labeled on the structures. (c) Overlays of the structures of apo pro-IL-18 (magenta) and pro-IL-18 complexed with caspase-1 (cyan) is shown. The dashed box highlights a region of significant structural difference between the two, which includes the β1 and β* strands. Residues 53−80, which include β* (55−58), are missing entirely from the structure of the complex and are presumably disordered in that state. Additionally, the I48 side chain, part of the β1 strand, resides in the core of the protein in the apo structure, while in the complex the side chain points to the solvent, where it forms an interaction with the side chain of W294 from caspase-1. Notably, there are substantial differences in the structures of pro- and mature IL-18, which have been described in detail previously.[19]

immune responses. As such, elevated levels of IL-18 have been implicated in a number of autoimmune diseases.[15,18]

Recently, we have published a solution NMR structure of pro-IL-18, as well as a cryo-EM structure of pro-IL-18 complexed with caspase-1 (Figure 1b).[19] A comparison of these structures reveals significant differences between the apo and complexed forms, particularly in the β1 and β* strands of the protein (Figure 1c), though both forms adopt a β trefoil fold. In particular, the side chain of I48 (β1), which forms a critical interaction with W294 of caspase-1 in the complex,[19] is buried in the core of the apo form. In addition, the residues forming β* in the apo form are not observed in the cryo-EM structure of the complex, presumably because they are disordered. The structural changes associated with binding of pro-IL-18 to caspase-1 and caspase-4 raise the question of whether the observed structural transitions might be facilitated by protein dynamics, in this case in the apo state, as has been seen in other systems.

Nuclear magnetic resonance (NMR) spectroscopy is a powerful tool for the characterization of protein motions, at atomic resolution, across a broad window of time scales. Here we have used a range of NMR techniques to quantify the dynamics of pro-IL-18 on time scales ranging from pico-seconds to days. We have recorded ^{15}N spin relaxation experiments that are only sensitive to pico- to nanosecond time scale motions, with contributions from slower time scale motions suppressed,[20] as well as Carr−Purcell−Meiboom−Gill (CPMG)[21−23] and chemical exchange saturation transfer (CEST)[24] data sets, that typically report on exchange time scales in the ∼0.2−10 ms[25] and ∼2−20 ms ranges,[24] respectively, measured on a variety of backbone and side chain methyl probes. Peak duplication is observed for multiple residues in ^{1}H−^{15}N correlation spectra of pro-IL-18, localized to Q92-P93 cis:trans peptide bond isomerization; such equilibria typically report dynamics on lifetimes in the many tens to hundreds of seconds. Finally, hydrogen−deuterium exchange (HDX) data sets, sensitive to dynamics on time scales that can extend to multiple days, have also been measured. The extensive range of time scales explored in this study provides an opportunity to address whether a hierarchy of motions and motional time scales is present in unbound pro-IL-18. Notably, in this regard, we find that the β1 and β* strands, while rigid on the ps−ns time scale, undergo exchange on the μs−ms time scale involving at least three conformational states that do not recapitulate the caspase-bound form. HDX data establish that these two strands participate in a further exchange process, in which they become unfolded in a sparsely formed state. The correlation between residues with

https://doi.org/10.1021/jacs.4c09805
J. Am. Chem. Soc. 2024, 146, 30281−30293

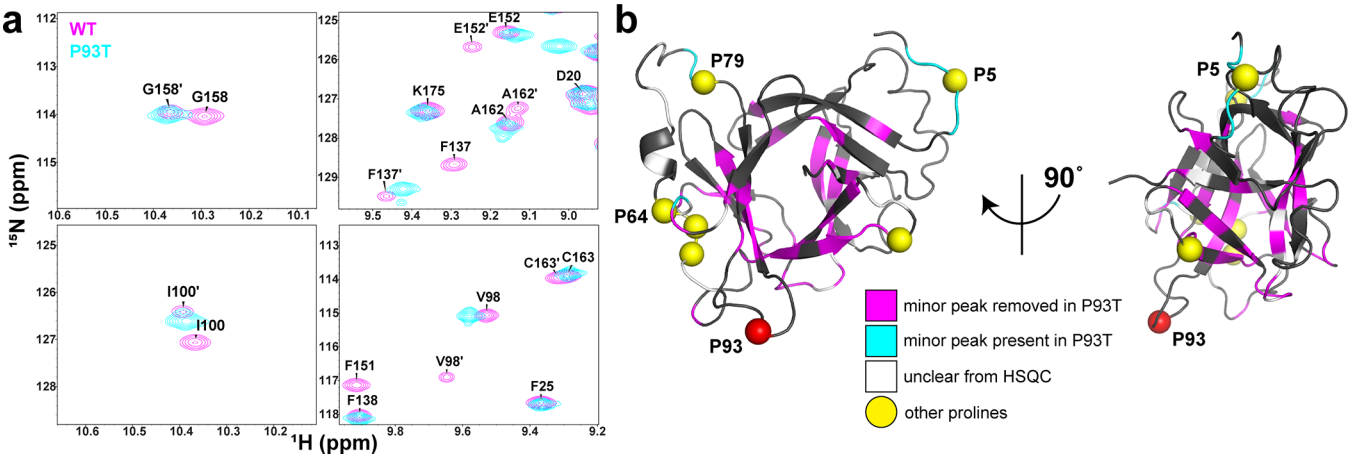

Figure 2. Two sets of peaks in ^{1}H−^{15}N spectra of pro-IL-18 stem from isomerization of the Q92-P93 peptide bond. (a) Overlays of selected regions from ^{1}H−^{15}N HSQC spectra of WT (magenta) and P93T (cyan) pro-IL-18 are shown. Assignments of peaks derived from the WT protein are displayed, with the minor state resonances indicated by ′. Nearly all of the residues with a minor peak in the WT spectrum have only a single peak in the P93T spectrum, indicating that these minor peaks result from a *cis*−*trans* isomerization of the Q92-P93 peptide bond. (b) Residues whose amide has a minor peak are shown on the structure of pro-IL-18. The seven prolines are indicated as spheres, with P93 colored in red. Residues whose minor peak is gone in the P93T spectrum are colored in magenta, while the few residues whose minor peak is still present in the P93T spectrum are colored in cyan. These residues cluster around other prolines (A3, E4, V6, and E7 around P5; N62 around P64; N77 and A78 around P79) and presumably stem from isomerization of these other prolines. Finally, residues whose minor peak status in P93T cannot be confidently determined by the HSQC due to spectral overlap are colored in white.

both μs−ms time scale dynamics and slower motions resulting in local unfolding in the apo protein and residues participating in the structural changes accompanying binding to caspase-1/-4 suggests that the plasticity of pro-IL-18 can play an important role in the maturation of this cytokine.

RESULTS AND DISCUSSION

Two Sets of Resonances in ^{1}H−^{15}N HSQC Spectra of Pro-IL-18 Stem from Isomerization of P93. Initial ^{1}H−^{15}N HSQC spectra recorded on pro-IL-18 revealed two sets of resonances for many amides (Figure 2a), for which the relative intensities are roughly 2:1. Notably, amides yielding two peaks are found for residues located all over the molecule, including all 13 strands of the β-trefoil (Figure 2b). Given that mature IL-18 is reported to also show two sets of amide resonances which result from an isomerization of P79,[26] we hypothesized that the second set of resonances observed in pro-IL-18 is also due to proline isomerization. Interestingly, mutation of each of the seven proline residues in pro-IL-18 (one at a time) revealed that while this second set of amide resonances is indeed due to proline isomerization, it is, in fact, P93 that is responsible rather than P79 as in the mature form (Figure 2a,b). Further, the ^{13}Cβ (31.7 ppm) and ^{13}Cγ (27.5 ppm) side chain chemical shifts of the major conformation of P93 are consistent with a *trans* Q92-P93 peptide bond for this state.[27] Notably, there are a few amides that still show a second resonance in P93T, which cluster around P5, P64, and P79, suggesting that both *cis* and *trans* forms of these prolines are also populated, though the structural consequences of these isomerization equilibria are localized, unlike that of P93 (Figure 2b). While a great number of probes throughout the protein structure are sensitive to the isomerization of the Q92-P93 peptide bond, the generally small chemical shift differences between the two sets of amide peaks in each case suggest that the structural changes induced by this isomerization event are small. The exchange process could not be further characterized through magnetization exchange experiments, which are sensitive to exchange processes on the order of several times per second (although we did try), as proline isomerization is typically in a time window of many tens of seconds or higher.[28] Nevertheless, the isomerization process observed for pro-IL-18, in particular, involving large segments of the protein, provides a first hint of a dynamic molecule, which we subsequently explore further below. It is worth noting that our study focuses on the major state (higher intensity signals), corresponding to the *trans* conformation of the Q92-P93 peptide bond.

β Strands of Pro-IL-18 Are Rigid on the ps−ns Time Scale. As described in the previous section, the Q92-P93 *cis*/*trans* peptide bond isomerization leads to additional peaks in NMR spectra that are derived from residues throughout all β-strands in pro-IL-18 (Figure 2b). Given this inherent plasticity, we wondered whether the strands might also show increased dynamics on additional time scales, including within the ps−ns window. Such fast motions have been shown to contribute significantly to the conformational entropy of proteins, which can play an important role in binding thermodynamics.[29] To rigorously characterize the dynamics of pro-IL-18 on this time scale, we have recorded a series of data sets that focus on relaxation of ^{1}H−^{15}N two spin elements, including ^{1}H−^{15}N longitudinal order, antiphase ^{1}H and ^{15}N single quantum coherences, and ^{1}H−^{15}N multiple quantum coherences,[20] in addition to traditional experiments that record ^{15}N in-phase $R_{1\rho}$ and R_1 relaxation rates, as well as ^{15}N{^{1}H}-heteronuclear NOEs.[30] The importance of the two-spin element experiments is underscored by the fact that from an appropriate linear combination of all four rates it is possible to obtain a measure of ^{15}N dipole−dipole transverse relaxation which is not contaminated by chemical exchange, R_{dd}.[20] Alternatively, from a different linear combination, the residual chemical exchange contribution to ^{15}N transverse magnetization under the experimental spin lock conditions, $R_{ex,\rho}$, can be estimated.[31] Values of a residue-specific spectral density function, $J(\omega)$, measuring the motion of the ^{1}H−^{15}N bond vector in question

https://doi.org/10.1021/jacs.4c09805
J. Am. Chem. Soc. 2024, 146, 30281−30293

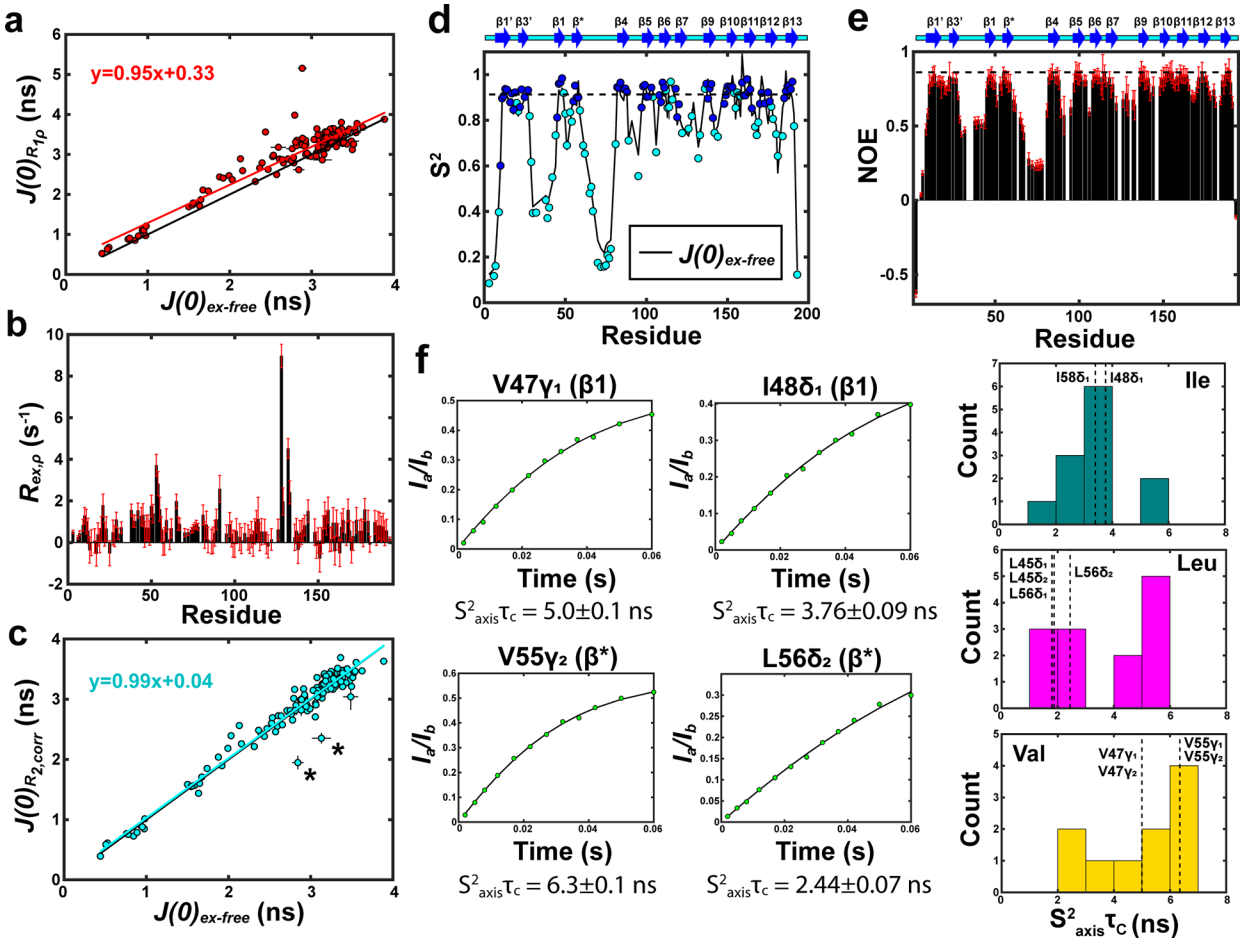

Figure 3. β strands of pro-IL-18 are rigid on the ps−ns time scale. (a) Comparison of $J(0)_{ex-free}$ and $J(0)_{R_{1\rho}}$, calculated from R_{dd} or from $R_{1\rho}$ derived R_2 rates, respectively, as described in the text. The best fit line is shown in red ($y = 0.95x + 0.33$), while the line $y = x$ is shown in black. (b) $R_{ex,\rho}$ as a function of residue number. Reported errors (red) also reflect the potential variation in residue specific chemical shift anisotropy values, as described previously.[31] (c) Comparison of $J(0)$ values calculated by spectral density mapping using $R_{2,corr} = R_2 - R_{ex,\rho}$, referred to as $J(0)_{R_{2,corr}}$ and $J(0)_{ex-free}$. The best fit line is shown in cyan ($y = 0.99x + 0.04$), while the line $y = x$ is shown in black. The two largest outliers, denoted by the asterisks, were omitted from the subsequent order parameter determination. The reason for these outliers is unclear presently. (d) Backbone amide bond vector order parameters as a function of residue number. Amides from residues in β strands are colored blue, while all other amides are shown in cyan. The black curve connects the $J(0)_{ex-free}$ values, scaled such that the agreement with the S^2 profile is highest. The dashed black line at $S^2 = 0.913$ marks the average order parameter of amides from all β strands. The secondary structure diagram shows the locations of all β strands in pro-IL-18. (e) Heteronuclear NOE as a function of residue number, with the dashed black line at NOE = 0.86 marking the theoretical maximum NOE value at 800 MHz for a molecule with an effective correlation time of pro-IL-18 (8.7 ns; 1.04 Å bond length and ^{15}N CSA of -163 ppm [49]). Error bars are included in all plots but can be smaller than the symbols used. (f) I_a/I_b as a function of time from a triple-quantum based relaxation violated coherence transfer experiment[34] is plotted for selected methyl groups within β1 and β* (circles) along with the best fit of the data (see Supporting Information). Error bars are smaller than the symbols. Histograms of $S^2_{axis}\tau_C$ values are shown for methyl groups of Ile, Leu, and Val residues in β strands, with the values for residues within β1 and β* marked by dashed vertical lines.

and evaluated at 0, ω_N, and $0.87\omega_H$ frequencies (ω_i is the Larmor frequency of nucleus i) were obtained from an analysis of either (R_{dd}, R_1,^{15}N{^{1}H}-NOE) or ($R_{1\rho}$,R_1,^{15}N{^{1}H}-NOE) parameters.[32] The resulting $J(0)$ values are of particular interest, since $J(0) \propto S^2\tau_C$, where S^2 is the square of an order parameter quantifying the amplitude of the motion of the amide bond vector, and τ_C is a residue specific correlation time that depends, upon other things, on the orientation of the amide bond with respect to the molecular diffusion tensor.[33] Note that $J(0)$ values obtained from R_{dd} are exchange free (referred to as $J(0)_{ex-free}$), while the second set of $J(0)$s, from $R_{1\rho}$ (referred to as $J(0)_{R_{1\rho}}$), can be contaminated with exchange. That this is the case is illustrated in Figure 3a, where for many of the residues, $J(0)_{R_{1\rho}} > J(0)_{ex-free}$, and in Figure 3b, which plots $R_{ex,\rho}$ vs residue. $R_{ex,\rho}$ values are nonzero for many amides, with several rates greater than 3 s^{-1} and the largest value of approximately 9 s^{-1}. Correcting the R_2 rates derived from $R_{1\rho}$, via the relation $R_{2,corr} = R_2 - R_{ex,\rho}$, and then repeating the spectral density mapping with these corrected transverse rates yielded $J(0)_{R_{2,corr}}$ values which are in good agreement with $J(0)_{ex-free}$ (Figure 3c). Values of S^2 were then calculated from ($R_{2,corr}$, R_1, ^{15}N{^{1}H}-NOE) after first estimating the diffusion tensor (see Materials & Methods); order parameters range between 0 and 1, where a value of 1 indicates that the amide is rigid, while a value of 0 is indicative of unrestricted motion on this fast time scale. Notably, all β strands of pro-IL-18, including β1 and β*, are rigid, with an average S^2 value calculated over all β strands of 0.91 ± 0.001. Further, the average heteronuclear NOE values in β strands are

https://doi.org/10.1021/jacs.4c09805
J. Am. Chem. Soc. 2024, 146, 30281−30293

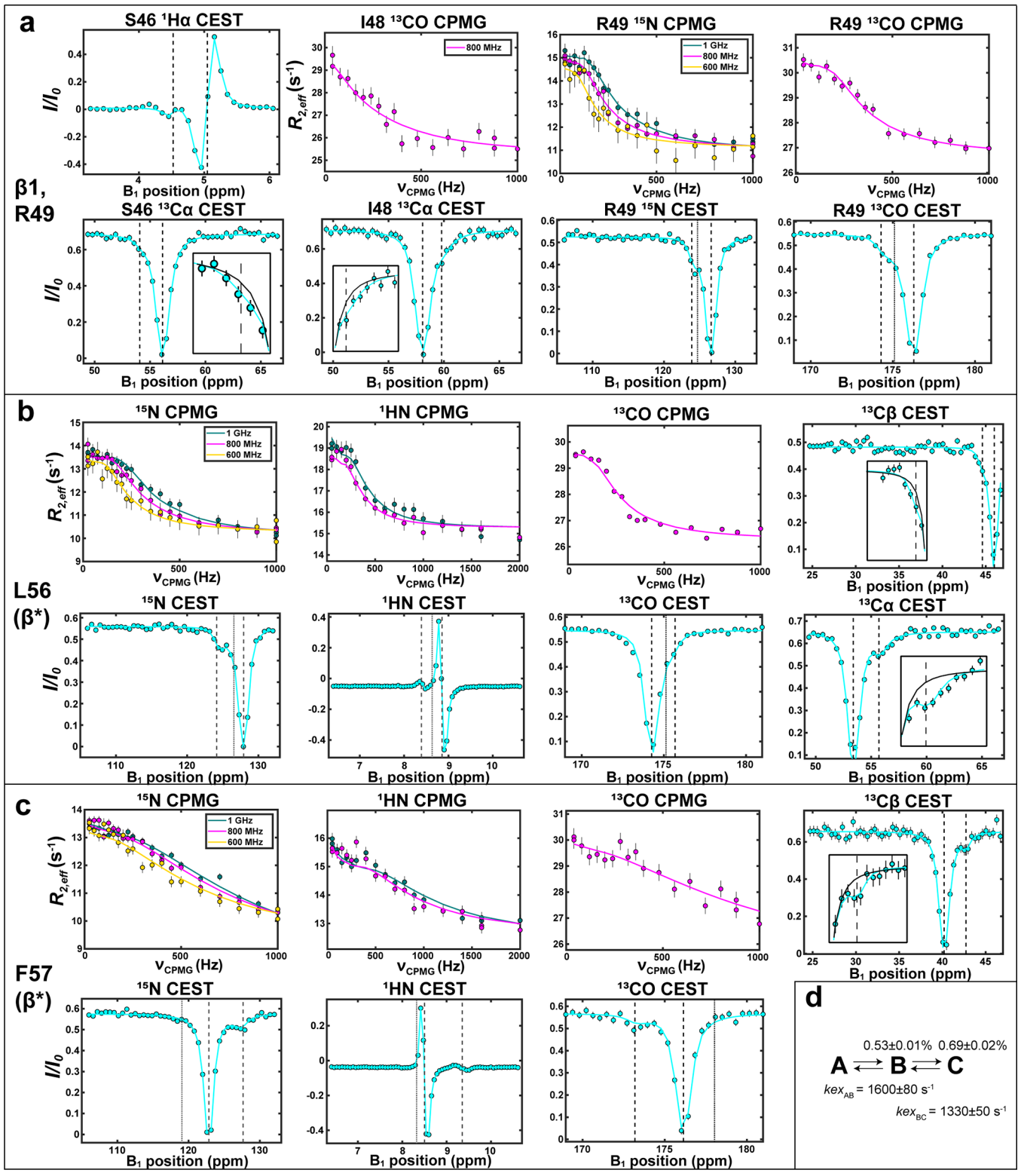

Figure 4. The μs−ms time scale backbone dynamics of pro-IL-18 can be described by a 3-state exchange model. CPMG and CEST profiles (circles) are shown for a number of nuclei from S46, I48 (both in β1), and R49 (a) as well as L56 (b) and F57 (c), both in β*. Superimposed on the profiles are fits to a linear 3-state model (solid lines). (d) Populations and exchange rates were determined from a combined fit of the ^{15}N CPMG and ^{15}N CEST data for all residues. The two dashed vertical lines on the CEST profiles indicate the chemical shifts of states A (ground state) and C (longer-lived excited state). The dotted line marks the chemical shift of state B. Dotted lines are not placed on the Cα, Cβ, and Hα profiles, as the lack of CPMG data for these nuclei precludes accurate determination of state B chemical shifts in these cases. Insets in panels show an overlay of the 3-state model fit (cyan) and a fit where exchange is not included (black), focusing on a region in the vicinity of the chemical shifts of residues in state C. In this and all following figures, CPMG profiles in overlays are shifted vertically such that the fit curves coincide at the last ν_{CPMG} value.

https://doi.org/10.1021/jacs.4c09805
J. Am. Chem. Soc. 2024, 146, 30281−30293

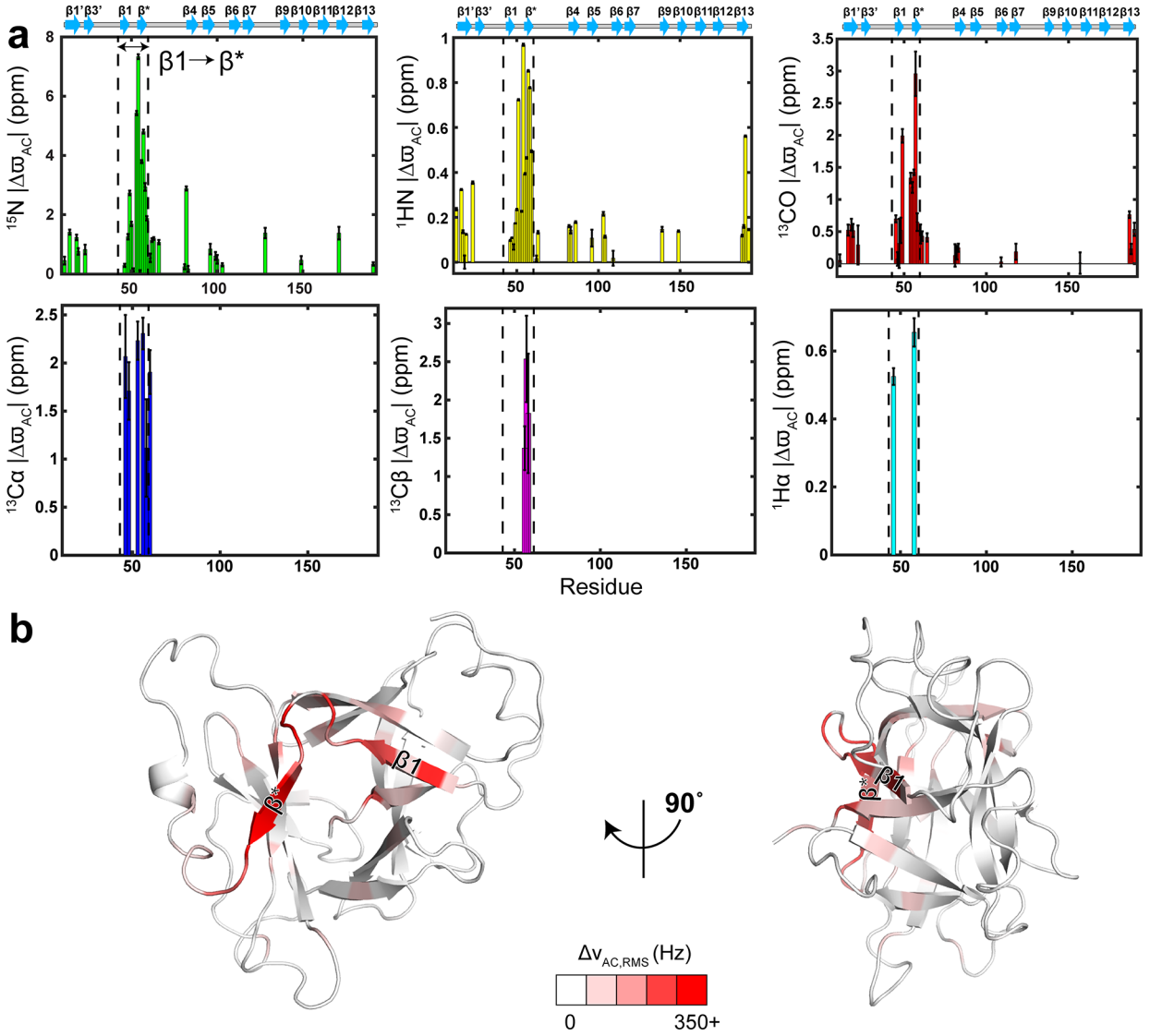

Figure 5. The largest structural differences between ground and excited states are in the $\beta1-\beta^*$ region. (a) The magnitude of $\Delta\varpi_{AC}$ for each residue is shown for ^{15}N, ^{1}HN, ^{13}CO, $^{13}C\alpha$, $^{13}C\beta$, and $^{1}H\alpha$ spins. The region from $\beta1$ to β^* (residues 45−58) is demarcated by dashed lines in each panel. (b) $\Delta\nu_{AC,RMS}$ values are displayed on the pro-IL-18 structure (PDB code 8URV)[19] as a white-red gradient, where $\Delta\nu_{AC,RMS} = \sqrt{\frac{1}{N}\sum_{i=1}^{N}\Delta\nu_{AC,i}^2}$ and $\Delta\nu_{AC,i}$ is the chemical shift difference of nucleus i in states A and C ($\nu_C - \nu_A$), in Hz. The largest $\Delta\nu_{AC,RMS}$ values are found in $\beta1$ and β^*, as well as in the turn bridging these two strands, suggesting that the largest structural differences between the ground and excited states occur in this region. The maximum value of $\Delta\nu_{AC,RMS}$ is close to 600 Hz for F57 (see Table S3), but the color gradient is cut off at 350 Hz for visual clarity.

close to the maximum value of 0.86 (800 MHz) that would be expected for pro-IL-18, again consistent with their rigidity on the ps−ns time scale.

To characterize the ps−ns dynamics of pro-IL-18 beyond the backbone, we also measured intramethyl $^{1}H-^{1}H$ dipolar cross-correlated relaxation rates of Ile, Leu, and Val side chain methyl groups via a triple-quantum based relaxation violated coherence transfer experiment.[34] Fits of the ratio of peak intensities resulting from the forbidden (I_a) and allowed (I_b) transitions, I_a/I_b (Figure 3f), enables the determination of the cross-correlated relaxation rate, which can then be used to calculate $S^2_{axis}\tau_C$, where S^2_{axis} is an order parameter squared describing the amplitude of motion of the methyl 3-fold axis.[35] While the methyl groups of L45 ($\beta1$) and L56 (β^*) have relatively low $S^2_{axis}\tau_C$ values compared to other Leu residues in β strands, the $S^2_{axis}\tau_C$ values measured for methyl groups of Ile and Val in $\beta1$ (V47, I48) and β^* (V55, I58) are typical of these residue-types throughout the β strands of pro-IL-18 (Figure 3f). Thus, on the picosecond to nanosecond time scale, $\beta1$ and β^* do not show unusual dynamics in relation to other β strands in pro-IL-18.

***β1* and *β** Are Dynamic on the *μ*s−ms Time Scale.** In contrast to localized motions observed in proteins on the ps−ns time scale, concerted motions involving many residues in a protein, in some cases related to ligand binding and enzyme catalysis, often occur on the μs−ms time scale.[3,12,36,37] The nonzero $R_{ex,\rho}$ rates discussed in the previous section indicate that pro-IL-18 is dynamic on this slower time scale. To characterize the dynamics of pro-IL-18 in the μs−ms motional regime, we collected CPMG data sets on three different backbone probes (^{15}N, ^{1}HN, ^{13}CO) as well as data sets focusing on Ile (δ_1), Leu (δ_1, δ_2), and Val (γ_1, γ_2) (ILV) side

https://doi.org/10.1021/jacs.4c09805
J. Am. Chem. Soc. 2024, 146, 30281−30293

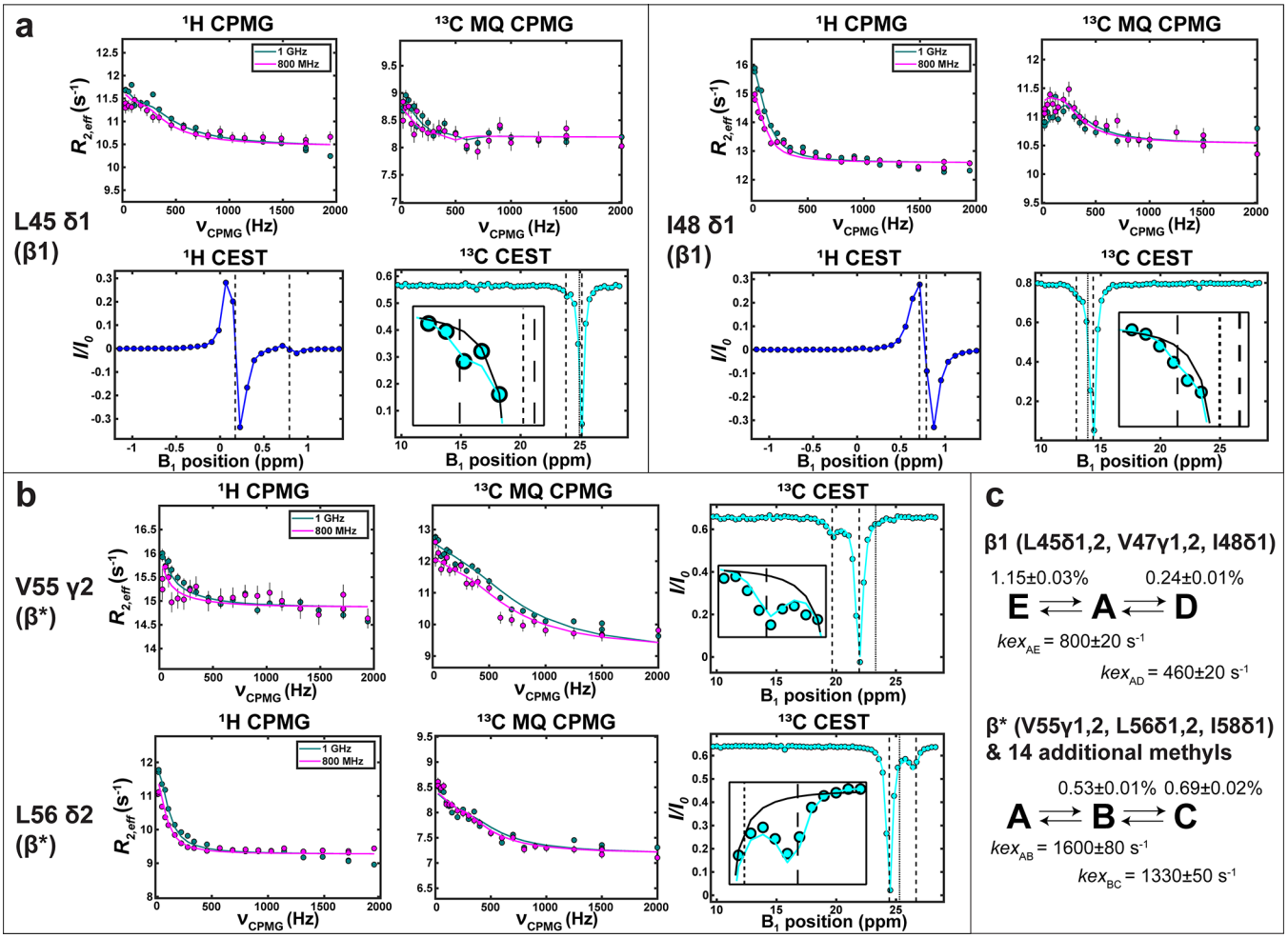

Figure 6. An additional ms time scale motional process is reported by the side chain methyl groups of β1. Methyl CPMG (^{13}C MQ and ^{1}H SQ) and CEST (^{1}H and ^{13}C) profiles are shown for several residues in β1 (a) and β* (b), along with fits to 3-state models. While the linear 3-state model determined from the backbone data produced good fits for the majority of the methyl group profiles (19 of 25 considered) (c), poor quality fits for the methyl groups of L45, V47, and I48 in β1 were observed. Instead, a bifurcated 3-state model best describes the data from these methyl groups (c). Vertical dashed lines on the CEST profiles indicate the chemical shifts of nuclei in states A (ground state) and either state C (V55, L56) or state D (L45, I48), while the dotted lines denote shifts of spins in state B or state E. Only chemical shifts of nuclei in state C or state D are fit from the ^{1}H profiles (i.e., no dotted lines; see Materials & Methods). The insets in ^{13}C CEST panels show an overlay of the 3-state model fit (cyan) and a fit assuming no chemical exchange (black) in a region proximal to the chemical shift of the nucleus in either state C or state D.

chain methyl ^{13}C and ^{1}H spins (Table S1). In addition, we recorded ^{15}N, ^{1}HN, ^{13}CO, ^{13}Cα, ^{13}Cβ, and ^{1}Hα CEST data sets as well as ^{13}C and ^{1}H ILV methyl group CEST profiles (Table S2). Initial attempts to analyze the ^{15}N CPMG and ^{15}N CEST data, independently, with a 2-state model on a per-residue basis revealed different populations and exchange rates for the same amide from the two methodologies (Figure S1), indicating that the true exchange kinetics are more complex. Global fits of the combined ^{15}N CPMG and ^{15}N CEST data to a triangular model led to significantly improved results. To simplify the analysis, we next considered both linear (A↔B↔C) and bifurcated (B↔A↔C) three-state models, where A denotes the major, observable conformer and B and C are the minor states, whose resonances are not observed in conventional ^{1}H−^{15}N or ^{1}H−^{13}C correlation spectra. Both schemes generally reproduced the CPMG and CEST data well; however, there were cases where the linear model yielded significantly better fits than the bifurcated model (Figure S2). Notably, the linear 3-state model enabled a global fit of the ^{15}N CPMG and ^{15}N CEST data from all exchanging residues, yielding minor state populations $p_B = 0.53 \pm 0.01\%$, $p_C = 0.69 \pm 0.02\%$, and exchange rates $k_{ex,AB} = 1600 \pm 80\ s^{-1}$, $k_{ex,BC} = 1330 \pm 50\ s^{-1}$ ($\chi^2_{red} = 0.8$), where $k_{ex,ij} = k_{ij} + k_{ji}$. In the analysis of the remaining backbone data, the populations and exchange rates were fixed to these values, and the resulting fits reproduced the data reasonably well ($\chi^2_{red} = 2.6$, 2.2, 0.9, 1.0, and 1.8 for ^{1}HN, ^{13}CO, ^{13}Cα, ^{13}Cβ, and ^{1}Hα, respectively) (Figure 4).

The lifetime of state C, $\tau_C = \frac{1}{k_{CB}} = 1.7$ ms, falls nicely within the CEST window, while the lifetime of state B, $\tau_B = \frac{1}{k_{BA} + k_{BC}} = 0.42$ ms, is approximately 4-fold shorter (i.e., faster exchange than optimal for CEST); thus, only minor state dips derived from state C are observed in CEST profiles. Further, CPMG profiles could not be recorded for ^{13}Cα, ^{13}Cβ, and ^{1}Hα probes due to interference effects resulting from homonuclear scalar couplings.[38,39] For these nuclei, only the (signed) chemical shift difference between the longer-lived excited state, state C, and state A ($\Delta\varpi_{AC} = \varpi_C - \varpi_A$, where ϖ is in ppm) could, therefore, be determined with reasonable accuracy (from the

https://doi.org/10.1021/jacs.4c09805
J. Am. Chem. Soc. 2024, 146, 30281−30293

CEST data). In what follows the more accurately defined $\Delta\varpi_{AC}$ values, that derive from the position of dips in CEST profiles, and include all the backbone and side chain $^{13}C\beta$ nuclei, are used in structural analyses, rather than $\Delta\varpi_{AB}$ shift differences, the latter of which are obtained only indirectly through analysis of CPMG data and do not include $^{13}C\alpha$, $^{13}C\beta$, and $^{1}H\alpha$ shifts that are important indicators of the type of secondary structure present. The large magnitude of $\Delta\varpi_{AC}$ (Figure 5a, Table S3) indicates that the relatively small exchange contribution to transverse relaxation observed in CPMG profiles (typically 4−5 s^{-1} or less) is the result of the small minor state populations. The largest chemical shift differences are seen in β1 and β*, as well as in the turn connecting them (Figure 5b). These strands show pronounced structural differences between apo pro-IL-18 and the complex between pro-IL-18 and either caspase-1[19] or caspase-4[16] (Figure 1c). Smaller ^{15}N, ^{1}HN, and ^{13}CO chemical shift changes are observed throughout $\beta1'$ and β13, the two strands sandwiching β1.

The combination of ^{15}N, ^{1}HN, ^{13}CO, $^{13}C\alpha$, $^{13}C\beta$, and $^{1}H\alpha$ chemical shifts enables the determination of regions of defined secondary structure in protein conformers, such as the excited state C considered here.[40−42] Of particular interest in the present study is the secondary structure of the region corresponding to β* in the ground state, as these residues are not observed in the cryo-EM structures of pro-IL-18 bound to caspase-1/-4 and are presumably disordered in either complex, and of β1 that changes position in the free and bound conformations. Using the chemical shift secondary structure population inference program (*CheSPI*),[43] we determined the secondary structure of these regions in both the ground (state A) and excited (state C) states (Table S4). Despite the large chemical shift differences observed across all of the backbone probes, regions corresponding to β1 and β* in the ground state remain in the β strand conformation in the excited state.

While the backbone analysis shows a concerted 3-state process shared by all exchanging residues, the side chain methyl data reveal some degree of heterogeneity in the μs−ms dynamics (Figure 6). The CPMG and CEST data from most of the methyl groups (19 of the 25 methyl groups for which relaxation data are available, Table S5) are fit well by the same linear 3-state model and parameters from the analysis of backbone probes, including methyl groups within the β* strand. However, the five methyls from β1 (L45, V47, and I48) showed distinct behavior as attempts to fit the ^{13}C methyl CEST data of V47 and I48, in particular, to the A↔B↔C model with parameters as determined from analysis of backbone data led to larger minor state dips in CEST profiles than were observed experimentally (Figure S3). Instead, the β1 methyl groups were fit well with a bifurcated 3-state model (E↔A↔D; excited states denoted by D and E to distinguish them from B and C in the linear model), where state D has a very small population of 0.24 ± 0.01% and large chemical shift differences, $\Delta\varpi_{AD}$ (Figure 6a,c, Table S5). Alternatively, the data could be fit to a 4-state model, D↔A↔B↔C (states A, B, C equivalent to those in the A↔B↔C scheme, described above), where the rates and populations related to states B and C are the same as those for the backbone (linear) model, with a similar χ^2_{red} to that obtained with the bifurcated 3-state model (and essentially identical parameters obtained for state D). Given that the data cannot discriminate between these two models, we present here the simpler 3-state model, although it may well be that the E↔A↔D process is, in fact, just a more complex version of the linear scheme (i.e., in reality D↔A↔B↔C, with E denoting B↔C). Notably, the fact that only five of the 25 methyl probes are sensitive to this distinct (or more complex) process, and that these are all proximal, suggests a local effect that influences only these side chains. Some insight into the nature of the structural changes that give rise to these additional conformers can be obtained by analysis of methyl ^{13}C chemical shifts in terms of side chain rotameric populations, as described below. However, detailed structural insights are not available from the limited data that include only methyl group chemical shifts. Similar to the backbone, the largest $\Delta\varpi$ values for the methyl groups are associated with β1 and β* (Figure 7). Sizeable shift changes are also observed in the adjacent strands β4 and β13.

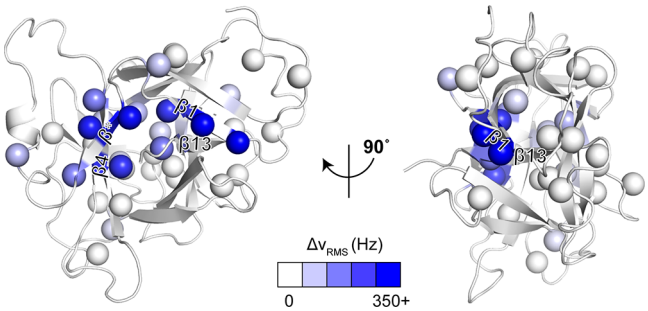

Figure 7. Significant chemical shift changes in β_1−β* region between ground and excited states as reported by side chain methyl groups. $\Delta\nu_{AC,RMS}$, $\Delta\nu_{AD,RMS}$, and $\Delta\nu_{AES1,RMS}$ for V189 ($\Delta\nu_{RMS}$) values are displayed on the pro-IL-18 structure (PDB code 8URV) as a white-blue gradient, with shift differences defined as in Figure 5 and including both geminal methyl groups from Leu and Val in the calculation (note that state C was used for all methyl groups in the calculation with the exception of those from β1 where $\Delta\nu_{AD,RMS}$ was calculated and V189 where state ES1 was used, Table S5C). The maximum value of $\Delta\nu_{RMS}$ is close to 500 Hz for L45 (see Table S5), but the color gradient is cut off at 350 Hz for visual clarity. Cβ carbons of Ile, Leu, and Val residues are shown in spheres. The largest $\Delta\nu_{AC,RMS}$ or $\Delta\nu_{AD,RMS}$ values are observed in β1 and β*, with methyl groups from nearby strands such as I82 (β4), I85 (β4), and V189 (β13) also showing noticeable shift differences.

Methyl ^{13}C chemical shifts of ILV residues correlate strongly with the rotameric states of these side chains. Using methods described previously,[44−46] we have determined the rotamer populations of ILV residues in β1 and β* in ground and excited states (Table S6). Interestingly, the χ2 angle of I48 (β1) shifts from nearly 100% *trans* in the ground state to a 2:1 ratio of *trans*:*gauche*(−) in the excited state (state D), consistent with increased motion and, hence, decreased packing around this side chain in the excited state. V55 (β*), whose $C\gamma_2$ lies only 4.3 Å from the $C\delta_1$ of I48, shows an even more dramatic shift from nearly 100% *trans* in the ground state to a 1:1 ratio of *trans*:*gauche*(−) in the excited state (state C). While the backbone data demonstrate that β1 and β* retain their secondary structure in the excited state, the methyl data show that the side chains of I48 and V55 become less restricted (Tables S6 and S7).

Probing Dynamics in β1 and β* via HDX. The chemical shift differences obtained from fits of the CPMG and CEST data sets are not consistent with local unfolding of strand β1 or β*. As discussed above, this is established through a combined analysis of backbone ^{1}H, ^{13}C, and ^{15}N chemical shifts using the *CheSPI* program where the population of random coil in these

https://doi.org/10.1021/jacs.4c09805
J. Am. Chem. Soc. 2024, 146, 30281−30293

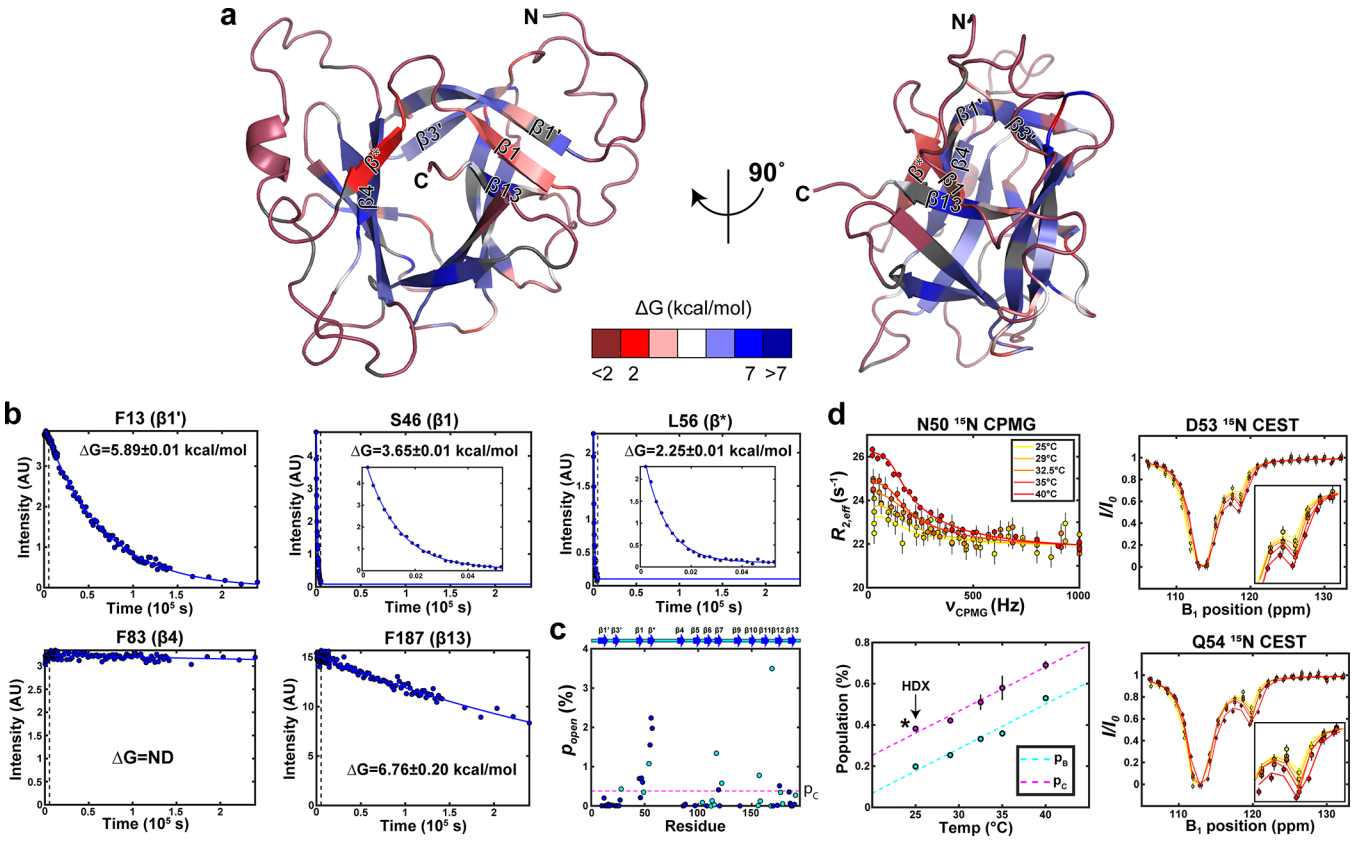

Figure 8. HDX NMR establishes an excited state where strands $\beta1$ and β^* locally unfold and reveals additional motion in the nearby $\beta1'$ and $\beta13$ strands. (a) ΔG values determined by HDX NMR are displayed on the structure of pro-IL-18 as a red-white-blue gradient ($\Delta G = -RT\ln(K_{open}) \approx -RT\ln(p_{open})$, where K_{open} is the equilibrium constant for the opening reaction to a rare exchange competent state of population p_{open}). Residues whose amide resonance intensity had already decayed to ∼0 in the first time point (210 s) are shown in the dark red color, while those whose amide resonance intensity decayed so little throughout the full time-course that a decay rate could not be fit are shown in the dark blue color. Finally, residues that could not be analyzed due to either peak overlap or lacking assignment are shown in gray. Several amides in β strands have low ΔG values, despite being hydrogen bonded, consistent with an exchange process involving unprotected conformations at these sites. These include β^* (L56), $\beta13$ (M186), $\beta10$ (M149), and most prominently $\beta1$, where all of the amides have low protection factors despite each being hydrogen bonded. Notably, $\beta13$ forms extensive contacts with $\beta1$, and the amide of M149 is hydrogen bonded to the carbonyl of V189 ($\beta13$). (b) Plots of intensity decays of amides from several β strands with fits to monoexponential decays shown. The dashed vertical lines mark the time point at which S46 and L56 have both essentially fully decayed (insets show zoomed-in regions of data up to this point in time). A range of ΔG values is observed, indicating that distinct unfolding motions are present in these various β strands. ΔG = ND (not determined) is given in cases where the intensity loss over the full time-course of the experiment is so small that a decay rate cannot be confidently determined. (c) Open (local unfolded) population is shown for all residues analyzed. Amides from residues in β strands are colored blue, and data for all other amides are shown in cyan. Error bars are within the data points. The horizontal dashed magenta line marks the population of state C at 25 °C determined by CPMG/CEST. (d) ^{15}N CPMG/CEST profiles and fits at 40, 35, 32.5, 29, and 25 °C are shown for several amides. The CEST profiles have been normalized by dividing each point by $\exp(-R_1 t)$, where R_1 is the ^{15}N longitudinal relaxation rate, and t is the duration of the CEST period. Excited state populations at each temperature are plotted, with dashed lines to guide the eye. At 25 °C, kex_{BC} was poorly defined by the data and so was fixed to the value obtained at 29 °C (this rate changes slowly with temperature; see Table S9). The resulting p_C (marked by an asterisk) follows the trend established at higher temperatures, indicating that this approximation is reasonable.

regions does not uniformly increase in the excited state C relative to the ground conformation (Table S4), and from a comparison of ^{1}HN and ^{15}N $\Delta\varpi_{AB}$ or $\Delta\varpi_{AC}$ values with $\Delta\varpi_{GD,RC}$ (random coil−ground state shifts) where state B and C shifts sometimes "moved" in a direction toward what would be expected for random coil and sometimes not (Figure S4). Nevertheless, the $\chi2$ and $\chi1$ torsion angles of I48 ($\beta1$) and V55 (β^*), respectively, transition from all *trans* (ground state) to approximately equal populations of *trans* and *gauche*(−) (states D and C) (Table S6), suggesting a loosening of the structure in the vicinity of I48, a key residue in stabilizing the pro-IL-18:caspase-1/-4 complex.[16,19] We, therefore, wondered if additional structural transitions involving $\beta1$ and β^* might be detected in a hydrogen exchange experiment which is sensitive to a range of motional time scales, including those slower than the μs−ms window that is relevant to CPMG and CEST.

To this end we carried out a hydrogen−deuterium exchange (HDX) NMR analysis, monitoring the disappearance of backbone amides in HSQC spectra recorded on samples where lyophilized protein was dissolved in D_2O. Here, experiments were performed at pD_{corr} = 5.85, 25 °C, as opposed to the conditions used for relaxation (pH = 6.5, 40 °C), in order to slow down the intrinsic rate of hydrogen exchange and hence ensure that exchange is in the EX2 regime.[47] In this way, the measured rates of hydrogen exchange are determined by the population of the "open" state rather than the kinetics of opening to an exchange competent

https://doi.org/10.1021/jacs.4c09805
J. Am. Chem. Soc. 2024, 146, 30281−30293

("excited") conformation. Thus, we report free energy values (related to populations of the excited state, p_{open}, via $\Delta G \approx -RT\ln(p_{open})$, where R and T are the gas constant and absolute temperature, respectively) for the dynamic processes observed but are unable to quantify the kinetics of the underlying motions driving the HDX exchange process (see below). The HDX data show rapid hydrogen exchange (i.e., a relatively large open population) in β1 and β* (Figure 8a−c). While the amides of V55 and F57 from β* are solvent exposed and are not hydrogen bonded in the NMR derived structure of pro-IL-18, the amide of L56 is hydrogen bonded to the carbonyl of F83 from β4.[19] Thus, the rapid hydrogen exchange observed for this residue is a clear indication of the dynamics in β*. The rapid hydrogen exchange observed in β1 is more striking as the backbone amide of each of the four residues of β1 forms a hydrogen bond with residues in β1′ or β13. The average open state populations obtained for β1 and β* are 0.55 ± 0.02% (n = 4) and 1.92 ± 0.02% (n = 3), respectively. Recall that it is unlikely that the relaxation and HDX approaches report on the same process(es), as the fitted chemical shift differences between states from CPMG/CEST data are not consistent with unfolding (see above).

To further demonstrate that the motions in β1 and β* detected by HDX and CPMG/CEST are distinct, we recorded additional ^{15}N CPMG and CEST data sets at 35, 32.5, 29, and 25 °C (Figure 8d), pH 6.5 (the pH used for recording the 40 °C relaxation data). We find that at 25 °C, p_B is reduced to just 0.2% and p_C is reduced to ≈0.4%. Additional CPMG experiments, recorded at pH 6.0 (roughly the pD used for HDX) establish that there are no significant changes in the populations of states B and C over the pH 6−6.5 range (Figure S5). Thus, the differences in populations of excited states observed via relaxation and hydrogen exchange experiments, particularly for β*, are consistent with each method reporting on separate excited states, as expected based on the $\Delta\varpi_{AB}$ and $\Delta\varpi_{AC}$ values which indicate that states B and C retain folded backbone conformations.

In addition to the rapid hydrogen exchange seen in β1 and β*, consistent with the local unfolding of these strands, we observed distinct open state populations in other β strands that do not correspond to global unfolding of the protein (Figure 8a,b). While most of the other β strands are almost entirely comprised of residues whose amides lose little to no intensity throughout the time course of the HDX experiment (F83 in Figure 8b, for example), every residue in β1′, β3′, and β13 exchanges to a significant degree. ΔG values obtained for hydrogen bonded residues in β1′ and β3′ (excluding the first and last residue of each strand) are quite uniform, with similar average values of 5.97 ± 0.01 kcal/mol (n = 4) and 5.89 ± 0.02 kcal/mol (n = 4), respectively (Table S8), corresponding to average open state populations of 0.0054 ± 0.0001% and 0.0050 ± 0.0002%, respectively. ΔG values in β13 are a bit more heterogeneous, with F187 and T188 values of 6.76 ± 0.20 kcal/mol (0.0011 ± 0.0003%) and 6.77 ± 0.04 kcal/mol (0.0011 ± 0.0001%), respectively, while M186 has a significantly lower free energy of 4.34 ± 0.01 kcal/mol (0.066 ± 0.001%). Thus, the HDX data reveal additional motional processes (local unfolding) that cannot be observed via CPMG/CEST, not only in strands β1 and β* but also in β1′, β3′, and β13. Notably, β1′ and β13 sandwich β1, raising the possibility that the motions of these three β-strands, leading to their observed hydrogen exchange dynamics, are all coupled.

CONCLUSION

IL-18 is an important regulator of the immune response. It functions through binding to cellular receptors, leading to the production of interferon-γ that in turn affects innate and adaptive immunity.[14] Like many other cytokines, IL-18 is produced in an inactive form (pro-IL-18) that must be enzymatically processed (in this case by caspase-1 or caspase-4) for maturation.[15,16] In a recent combined NMR/cryo-EM study we noted significant differences between the apo- and caspase-1 bound structures of pro-IL-18, including a small region that was in a β-strand conformation in the unbound structure, while unfolded in the complex (so-called β*, Figure 1c), and a second β-strand (β1) that is repositioned in the bound structure.[19] Notably, the pro-IL-18:caspase-1/-4 complex is stabilized through interactions at a pair of surfaces, one centered at the active site and a second distal region termed an exosite, where a key contact is formed between I48 of pro-IL-18 and W294/W267 of caspase-1/-4 (Figure 1c). The importance of interactions at the exosite is underscored by the fact that mutation of V47 and I48 results in impaired binding of pro-IL-18 to caspases-1 and -4, particularly to caspase-4.[16,19] I48 undergoes a significant structural transition, whereby it is buried in the interior of pro-IL-18 in the apo state yet flips out to interact with caspase-1/-4 in the complex. We wondered whether the significant structural changes accompanying caspase-1 binding might be facilitated by the intrinsic dynamics of apo pro-IL-18. Indeed, an excess number of peaks over what would be expected for a protein of 193 amino acids is observed in the ^{1}H−^{15}N HSQC fingerprint spectrum, attributed to a Q92-P93 cis−trans equilibrium (Figure 2b). Further, pairs of peaks associated with this transition were observed throughout pro-IL-18, including the majority of the β-strand core region (Figure 2b), hinting at a plastic structure whereby perturbations can be propagated throughout the molecule.

With this in mind, we performed a range of dynamics experiments that are sensitive to motions extending over 12 orders of magnitude, from picoseconds to nanoseconds to days. Care was taken to ensure that chemical exchange does not adversely affect the quantitation of backbone order parameters by recording experiments that rigorously eliminate such effects. Although all the β-strands in pro-IL-18 showed similar degrees of order on the ps−ns time scale, CPMG and CEST experiments (μs−ms time window), focusing on ^{1}H, ^{13}C, and ^{15}N backbone nuclei, ^{13}Cβ nuclei (CEST), as well as additional experiments based on methyl ^{1}H and ^{13}C spin probes, provided clear evidence for dynamics in strands β1 and β* that are more extensive than what is observed in other regions of the protein. Chemical shift differences between the major pro-IL-18 ground state and the sparsely populated pair of excited state conformers that were necessary for a global fit of the dispersion and CEST data were not consistent with local unfolding events in these regions but rather suggested more subtle rearrangements where the secondary structure was preserved (Table S7). Interestingly, changes in the distribution of side chain torsion angles for I48 and V55 that accompany the ground to excited D and C state transitions, respectively, suggest increased flexibility of the side chains of these residues (and hence potentially less packing) in these excited states, that may be significant in facilitating the transition of the I48 side chain from a buried state to a flipped-out conformation that stabilizes the caspase-1/-4 bound complex. The temper-

https://doi.org/10.1021/jacs.4c09805
J. Am. Chem. Soc. 2024, 146, 30281−30293

ature dependencies of the populations of states B and C also support the notion of less packed excited states relative to the ground conformer, A. Plots of $\ln(p_i)$ vs $1/T$ are linear (assuming temperature independent $\Delta H_{Ai} = H_i - H_A$ and $\Delta S_{Ai} = S_i - S_A$ values) with a slope of $-\Delta H_{Ai}/R$ and y-intercept of $\Delta S_{Ai}/R$ (Figure S6). Values of ΔH_{Ai} ($T\Delta S_{Ai}$, T = 313 K) so obtained, 11.9 ± 0.5 kcal/mol (8.7 ± 0.5 kcal/mol) and 7.7 ± 0.4 kcal/mol (4.6 ± 0.4 kcal/mol) for i = B and C, respectively, indicate enthalpically unfavorable and entropically favorable transitions from the ground state that are consistent with, but do not prove, weakening of intramolecular contacts. Finally, although local unfolding of β1 and β* could not be detected via analysis of our CPMG and CEST data, HDX-based experiments clearly establish the formation of at least one excited state (population of approximately 0.5−2%) where both of these strands are unfolded or at least significantly less stable relative to the ground conformer. These "unfolding" transitions occur on different time scales (very likely slower) than motions observable through dispersion and CEST techniques since they are not detected using these relaxation experiments. The unfolding of β1, as established through HDX measurements, may ultimately be required to accommodate the large changes in the backbone dihedral (ψ) angles of V47 (change in ψ of 178.3°) and R49 (58.7°) that lead to the flipped-out conformation of the I48 side chain which is a critical structural change for processing of the nascent IL-18 molecule (Figure 1c). In addition, the unfolding of β*, also observed via the HDX measurements described above, is inferred to occur in the pro-IL-18 complexes with caspase-1 and -4, based on the absence of these residues from both structures. Although the importance of unfolding of the β* strand to the structural transitions accompanying pro-IL-18:caspase-1/-4 formation is less clear, it is likely that the additional conformational flexibility in the region proximal to β1 (i.e., β*) could help facilitate the necessary transitions that occur upon pro-IL-18 binding to the caspase target.

A hierarchy of time scales in protein dynamics has been observed in connection with the function of adenylate kinase involving coupling of ps−ns motions in hinge regions with μs−ms motions that are required for lid opening of the enzyme.[11] A study by McDonald et al. revealed a more complex relationship between ps−ns and μs−ms dynamics in CheY, whereby colocalized changes in side chain flexibility on the ps−ns time scale (both increases and decreases in flexibility) accompany suppression of μs−ms motion upon phosphorylation.[48] Our data, however, suggest a lack of coupling between ps−ns and μs−ms motions for strands β1 and β*, yet are consistent with a hierarchy of dynamic processes linking ms time scale conformational changes of backbone structure and decreased packing of I48, a key residue for interacting with target caspases, with slower events involving local unfolding of strands β1 and β* of apo pro-IL-18. In this manner, these strands become "primed" for undergoing the structural changes that ultimately accompany binding to caspases-1 and -4. Our data paint a picture of a dynamic pro-IL-18 molecule whereby a range of motions covering different time scales facilitate binding to an enzymatic target to produce a functional mature state of the protein.

■ ASSOCIATED CONTENT

Data Availability Statement

The processed NMR data sets underlying this study are openly available in Zenodo at 10.5281/zenodo.12765510.

Supporting Information

The Supporting Information is available free of charge at https://pubs.acs.org/doi/10.1021/jacs.4c09805.

Materials and methods, tables containing details of CPMG/CEST experimental setup, fit parameter values from CPMG/CEST and HDX analyses, structural descriptions of the μs−ms time scale excited states, figures supporting the use of the linear 3-state model for CPMG/CEST analysis, the use of a distinct kinetic model for the methyl groups of β1, disagreement between ^{1}HN and ^{15}N $\Delta\varpi_{AB}$ and $\Delta\varpi_{AC}$ with $\Delta\varpi_{GD,RC}$, similarity of minor state populations at pH 6.5 and 6.0, and thermodynamic parameters of the exchange processes detected in the CPMG/CEST experiments (PDF)

■ AUTHOR INFORMATION

Corresponding Authors

Jeffrey P. Bonin − *Departments of Molecular Genetics and Biochemistry, University of Toronto, Toronto, Ontario M5S 1A8, Canada; Department of Chemistry, University of Toronto, Toronto, Ontario M5S 3H6, Canada; Program in Molecular Medicine, The Hospital for Sick Children Research Institute, Toronto, Ontario M5G 0A4, Canada*; Email: jeff.bonin@utoronto.ca

Lewis E. Kay − *Departments of Molecular Genetics and Biochemistry, University of Toronto, Toronto, Ontario M5S 1A8, Canada; Department of Chemistry, University of Toronto, Toronto, Ontario M5S 3H6, Canada; Program in Molecular Medicine, The Hospital for Sick Children Research Institute, Toronto, Ontario M5G 0A4, Canada*; orcid.org/0000-0002-4054-4083; Email: lewis.kay@utoronto.ca

Author

James M. Aramini − *Departments of Molecular Genetics and Biochemistry, University of Toronto, Toronto, Ontario M5S 1A8, Canada*

Complete contact information is available at: https://pubs.acs.org/10.1021/jacs.4c09805

Notes

The authors declare no competing financial interest.

■ ACKNOWLEDGMENTS

This work was supported through grants from the Canadian Institutes of Health Research (Grant FND-503573) and the Natural Sciences and Engineering Council of Canada (Grant 2015-04347) to L.E.K.

■ REFERENCES

(1) Henzler-Wildman, K.; Kern, D. Dynamic Personalities of Proteins. *Nature* **2007**, *450* (7172), 964−972.

(2) Karplus, M.; Kuriyan, J. Molecular Dynamics and Protein Function. *Proc. Natl. Acad. Sci. U. S. A.* **2005**, *102* (19), 6679−6685.

(3) Beach, H.; Cole, R.; Gill, M. L.; Loria, J. P. Conservation of Ms−ms Enzyme Motions in the Apo- and Substrate-Mimicked State. *J. Am. Chem. Soc.* **2005**, *127* (25), 9167−9176.

(4) Petit, C. M.; Zhang, J.; Sapienza, P. J.; Fuentes, E. J.; Lee, A. L. Hidden Dynamic Allostery in a PDZ Domain. *Proc. Natl. Acad. Sci. U. S. A.* **2009**, *106* (43), 18249−18254.

(5) Tzeng, S.-R.; Kalodimos, C. G. Allosteric Inhibition through Suppression of Transient Conformational States. *Nat. Chem. Biol.* **2013**, *9* (7), 462−465.
(6) Sekhar, A.; Kay, L. E. NMR Paves the Way for Atomic Level Descriptions of Sparsely Populated, Transiently Formed Biomolecular Conformers. *Proc. Natl. Acad. Sci. U. S. A.* **2013**, *110* (32), 12867−12874.
(7) Otten, R.; Liu, L.; Kenner, L. R.; Clarkson, M. W.; Mavor, D.; Tawfik, D. S.; Kern, D.; Fraser, J. S. Rescue of Conformational Dynamics in Enzyme Catalysis by Directed Evolution. *Nat. Commun.* **2018**, *9* (1), 1314.
(8) Whittier, S. K.; Hengge, A. C.; Loria, J. P. Conformational Motions Regulate Phosphoryl Transfer in Related Protein Tyrosine Phosphatases. *Science (1979)* **2013**, *341* (6148), 899−903.
(9) Xie, T.; Saleh, T.; Rossi, P.; Kalodimos, C. G. Conformational States Dynamically Populated by a Kinase Determine Its Function. *Science* **2020**, *370* (6513), eabc2754.
(10) Fraser, J. S.; Clarkson, M. W.; Degnan, S. C.; Erion, R.; Kern, D.; Alber, T. Hidden Alternative Structures of Proline Isomerase Essential for Catalysis. *Nature* **2009**, *462* (7273), 669−673.
(11) Henzler-Wildman, K. A.; Lei, M.; Thai, V.; Kerns, S. J.; Karplus, M.; Kern, D. A Hierarchy of Timescales in Protein Dynamics Is Linked to Enzyme Catalysis. *Nature* **2007**, *450* (7171), 913−916.
(12) Boehr, D. D.; McElheny, D.; Dyson, H. J.; Wright, P. E. The Dynamic Energy Landscape of Dihydrofolate Reductase Catalysis. *Science (1979)* **2006**, *313* (5793), 1638−1642.
(13) Culik, R. M.; Sekhar, A.; Nagesh, J.; Deol, H.; Rumfeldt, J. A. O.; Meiering, E. M.; Kay, L. E. Effects of Maturation on the Conformational Free-Energy Landscape of SOD1. *Proc. Natl. Acad. Sci. U. S. A.* **2018**, *115* (11), E2546.
(14) Garlanda, C.; Dinarello, C. A.; Mantovani, A. The Interleukin-1 Family: Back to the Future. *Immunity* **2013**, *39* (6), 1003−1018.
(15) Kaplanski, G. Interleukin-18: Biological Properties and Role in Disease Pathogenesis. *Immunol Rev.* **2018**, *281* (1), 138−153.
(16) Devant, P.; Dong, Y.; Mintseris, J.; Ma, W.; Gygi, S. P.; Wu, H.; Kagan, J. C. Structural Insights into Cytokine Cleavage by Inflammatory Caspase-4. *Nature* **2023**, *624* (7991), 451−459.
(17) Yasuda, K.; Nakanishi, K.; Tsutsui, H. Interleukin-18 in Health and Disease. *Int. J. Mol. Sci.* **2019**, *20* (3), 649.
(18) Ihim, S. A.; Abubakar, S. D.; Zian, Z.; Sasaki, T.; Saffarioun, M.; Maleknia, S.; Azizi, G. Interleukin-18 Cytokine in Immunity, Inflammation, and Autoimmunity: Biological Role in Induction, Regulation, and Treatment. *Front Immunol* **2022**, *13*, No. 919973.
(19) Dong, Y.; Bonin, J. P.; Devant, P.; Liang, Z.; Sever, A. I. M.; Mintseris, J.; Aramini, J. M.; Du, G.; Gygi, S. P.; Kagan, J. C.; Kay, L. E.; Wu, H. Structural Transitions Enable Interleukin-18 Maturation and Signaling. *Immunity* **2024**, *57* (7), 1533−1548.
(20) Hansen, D. F.; Yang, D.; Feng, H.; Zhou, Z.; Wiesner, S.; Bai, Y.; Kay, L. E. An Exchange-Free Measure of ^{15}N Transverse Relaxation: An NMR Spectroscopy Application to the Study of a Folding Intermediate with Pervasive Chemical Exchange. *J. Am. Chem. Soc.* **2007**, *129* (37), 11468−11479.
(21) Carr, H. Y.; Purcell, E. M. Effects of Diffusion on Free Precession in Nuclear Magnetic Resonance Experiments. *Phys. Rev.* **1954**, *94* (3), 630−638.
(22) Meiboom, S.; Gill, D. Modified Spin-Echo Method for Measuring Nuclear Relaxation Times. *Rev. Sci. Instrum.* **1958**, *29* (8), 688−691.
(23) Palmer, A. G.; Kroenke, C. D.; Patrick Loria, J. *Nuclear Magnetic Resonance Methods for Quantifying Microsecond-to-Millisecond Motions in Biological Macromolecules* **2001**, *339*, 204−238.
(24) Vallurupalli, P.; Bouvignies, G.; Kay, L. E. Studying "Invisible" Excited Protein States in Slow Exchange with a Major State Conformation. *J. Am. Chem. Soc.* **2012**, *134* (19), 8148−8161.
(25) Kleckner, I. R.; Foster, M. P. An Introduction to NMR-Based Approaches for Measuring Protein Dynamics. *Biochimica et Biophysica Acta (BBA) - Proteins and Proteomics* **2011**, *1814* (8), 942−968.
(26) Tsutsumi, N.; Kimura, T.; Arita, K.; Ariyoshi, M.; Ohnishi, H.; Yamamoto, T.; Zuo, X.; Maenaka, K.; Park, E. Y.; Kondo, N.; Shirakawa, M.; Tochio, H.; Kato, Z. The Structural Basis for Receptor Recognition of Human Interleukin-18. *Nat. Commun.* **2014**, *5* (1), 5340.
(27) Schubert, M.; Labudde, D.; Oschkinat, H.; Schmieder, P. A. Software Tool for the Prediction of Xaa-Pro Peptide Bond Conformations in Proteins Based on 13C Chemical Shift Statistics. *J. Biomol NMR* **2002**, *24* (2), 149−154.
(28) Grathwohl, C.; Wüthrich, K. Nmr Studies of the Rates of Proline Cis − Trans Isomerization in Oligopeptides. *Biopolymers* **1981**, *20* (12), 2623−2633.
(29) Wand, A. J.; Sharp, K. A. Measuring Entropy in Molecular Recognition by Proteins. *Annu. Rev. Biophys* **2018**, *47* (1), 41−61.
(30) Farrow, N. A.; Muhandiram, R.; Singer, A. U.; Pascal, S. M.; Kay, C. M.; Gish, G.; Shoelson, S. E.; Pawson, T.; Forman-Kay, J. D.; Kay, L. E. Backbone Dynamics of a Free and a Phosphopeptide-Complexed Src Homology 2 Domain Studied by 15N NMR Relaxation. *Biochemistry* **1994**, *33* (19), 5984−6003.
(31) Hansen, D. F.; Feng, H.; Zhou, Z.; Bai, Y.; Kay, L. E. Selective Characterization of Microsecond Motions in Proteins by NMR Relaxation. *J. Am. Chem. Soc.* **2009**, *131* (44), 16257−16265.
(32) Farrow, N. A.; Zhang, O.; Szabo, A.; Torchia, D. A.; Kay, L. E. Spectral Density Function Mapping Using 15N Relaxation Data Exclusively. *J. Biomol NMR* **1995**, *6* (2), 153−162.
(33) Tjandra, N.; Feller, S. E.; Pastor, R. W.; Bax, A. Rotational Diffusion Anisotropy of Human Ubiquitin from 15N NMR Relaxation. *J. Am. Chem. Soc.* **1995**, *117* (50), 12562−12566.
(34) Sun, H.; Kay, L. E.; Tugarinov, V. An Optimized Relaxation-Based Coherence Transfer NMR Experiment for the Measurement of Side-Chain Order in Methyl-Protonated, Highly Deuterated Proteins. *J. Phys. Chem. B* **2011**, *115* (49), 14878−14884.
(35) Kay, L. E.; Torchia, D. A. The Effects of Dipolar Cross Correlation on 13C Methyl-Carbon T1, T2, and NOE Measurements in Macromolecules. *Journal of Magnetic Resonance (1969)* **1991**, *95* (3), 536−547.
(36) Alderson, T. R.; Kay, L. E. Unveiling Invisible Protein States with NMR Spectroscopy. *Curr. Opin Struct Biol.* **2020**, *60*, 39−49.
(37) Sapienza, P. J.; Bonin, J. P.; Jinasena, H. P. D.; Li, K.; Dieckhaus, H.; Popov, K. I.; Aubé, J.; Lee, A. L. Mixed, Nonclassical Behavior in a Classic Allosteric Protein. *Proc. Natl. Acad. Sci. U. S. A.* **2023**, *120* (38), e2308338120.
(38) Vallurupalli, P.; Bouvignies, G.; Kay, L. E. A Computational Study of the Effects of 13C− 13C Scalar Couplings on 13C CEST NMR Spectra: Towards Studies on a Uniformly 13C-Labeled Protein. *ChemBioChem* **2013**, *14* (14), 1709−1713.
(39) Bouvignies, G.; Vallurupalli, P.; Kay, L. E. Visualizing Side Chains of Invisible Protein Conformers by Solution NMR. *J. Mol. Biol.* **2014**, *426* (3), 763−774.
(40) Wishart, D. S.; Sykes, B. D.; Richards, F. M. Relationship between Nuclear Magnetic Resonance Chemical Shift and Protein Secondary Structure. *J. Mol. Biol.* **1991**, *222* (2), 311−333.
(41) Shen, Y.; Bax, A. Protein Backbone and Sidechain Torsion Angles Predicted from NMR Chemical Shifts Using Artificial Neural Networks. *J. Biomol NMR* **2013**, *56* (3), 227−241.
(42) Shen, Y.; Bax, A. Protein Backbone Chemical Shifts Predicted from Searching a Database for Torsion Angle and Sequence Homology. *J. Biomol NMR* **2007**, *38* (4), 289−302.
(43) Nielsen, J. T.; Mulder, F. A. A. CheSPI: Chemical Shift Secondary Structure Population Inference. *J. Biomol NMR* **2021**, *75* (6−7), 273−291.
(44) Hansen, D. F.; Kay, L. E. Determining Valine Side-Chain Rotamer Conformations in Proteins from Methyl ^{13}C Chemical Shifts: Application to the 360 KDa Half-Proteasome. *J. Am. Chem. Soc.* **2011**, *133* (21), 8272−8281.
(45) Hansen, D. F.; Neudecker, P.; Kay, L. E. Determination of Isoleucine Side-Chain Conformations in Ground and Excited States of Proteins from Chemical Shifts. *J. Am. Chem. Soc.* **2010**, *132* (22), 7589−7591.
(46) Hansen, D. F.; Neudecker, P.; Vallurupalli, P.; Mulder, F. A. A.; Kay, L. E. Determination of Leu Side-Chain Conformations in Excited

Protein States by NMR Relaxation Dispersion. *J. Am. Chem. Soc.* **2010**, *132* (1), 42−43.
(47) Ferraro, D. M.; Lazo, N. D.; Robertson, A. D. EX1 Hydrogen Exchange and Protein Folding. *Biochemistry* **2004**, *43* (3), 587−594.
(48) McDonald, L. R.; Whitley, M. J.; Boyer, J. A.; Lee, A. L. Colocalization of Fast and Slow Timescale Dynamics in the Allosteric Signaling Protein CheY. *J. Mol. Biol.* **2013**, *425* (13), 2372−2381.
(49) Cornilescu, G.; Bax, A. Measurement of Proton, Nitrogen, and Carbonyl Chemical Shielding Anisotropies in a Protein Dissolved in a Dilute Liquid Crystalline Phase. *J. Am. Chem. Soc.* **2000**, *122* (41), 10143−10154.

https://doi.org/10.1021/jacs.4c09805
J. Am. Chem. Soc. 2024, 146, 30281−30293